Desalination and Water Treatment
www.deswater.com
doi: 10.1080/19443994.2013.873353

53 (2015) 3491–3498
March

Taylor & Francis
Taylor & Francis Group

Investigation of calcium carbonate precipitation in the presence of fluorescent-tagged scale inhibitor for cooling water systems

Huchuan Wang[a], Yuming Zhou[a,b,*], Guangqing Liu[a,d], Jingyi Huang[a], Qingzhao Yao[a,b], Shuaishuai Ma[a], Ke Cao[a], Yahui Liu[a], Wendao Wu[c], Wei Sun[c], Zhengjun Hu[c]

[a]*School of Chemistry and Chemical Engineering, Southeast University, Nanjing 211189, P.R. China*
[b]*Jiangsu Optoelectronic Functional Materials and Engineering Laboratory, Nanjing 211189, P.R. China*
Tel. +86 25 52090617; *email:* ymzhou@seu.edu.cn
[c]*Jianghai Environmental Protection Co. Ltd, Changzhou 213116, Jiangsu, P.R. China*
[d]*School of Biochemical and Environmental Engineering, Nanjing Xiaozhuang University, Nanjing 211171, P.R. China*

Received 28 July 2013; Accepted 3 December 2013

ABSTRACT

The aim of this work is to study the effect of a water-soluble copolymer, Acrylic acid–Oxalic acid–Allypolyethoxy carboxylate–8-hydroxy-1,3,6-pyrene trisulfonic acid trisodium salt (pyranine) (AA-APEM-APTA), APEM, and APTA were copolymerized with acrylic acid (AA) to synthesize APTA-tagged no phosphate and nitrogen-free $CaCO_3$ inhibitor, AA-APEM-APTA. Structures of APTA, APEM, and AA-APEM-APTA were carried out by FT–IR. The observation shows that the dosage of AA-APEM-APTA plays an important role on $CaCO_3$ inhibition. It can be concluded that the order of preventing the precipitation from flask tests was AA-APEM > AA-APEM-APTA > HPMA > PAA≈PESA. Relationship between AA-APEM-APTA's fluorescent intensity and its dosage was studied. Correlation coefficient r of AA-APEM-APTA's is 0.99672. The effect on the formation of $CaCO_3$ was investigated with combination of scanning electronic microscopy, transmission electron microscope, and X-ray powder diffraction analysis. AA-APEM-APTA can be used to accurately measure polymer consumption on line besides providing excellent $CaCO_3$.

Keywords: Calcium carbonate; Fluorescent-tagged; Scale inhibitor; Cooling water systems

1. Introduction

Circulating cooling water system is widely used in industrial processes because of its high water upkeep efficiency and rejection of thermal pollution of receiving water compared to once through cooling water system [1,2]. In this processes, scale problems occur on the surface of the facilities, essentially made up of $CaCO_3$, which could cause a total or partial obstruction of pipes and decrease the heat transfer, and even make the boiler burst [3–7]. The most common and effective method of scale controlling is the use of chemical additives as scale inhibitors that retard or prevent scale formation even in very small concentrations [8,9]. There are many classes of chemicals used as scale inhibitors to prevent scale formation. These are water-soluble molecules or polymers with several functional groups;

*Corresponding author.

the most common groups being phosphonate, carboxylate, and sulfonate.

Although the phosphonate and sulfonate containing scale inhibitor are highly efficient as a scale inhibitor, they have some fatal flaws such as difficult biodegradation in the water and eutrophication of the phosphorus-containing scale inhibitor. In addition, phosphonates, when reverted to orthophosphates, are potential nutrients for algae [10]. Recently, Kessler reported a novel non-phosphorus scale inhibitor. It is acrylic acid (AA)/ammonium allylpolyethoxy sulfate (APES) copolymer [11–13]. However, it is quite difficult to test for AA-APES by traditional way because there is no phosphate active component in it. Another defect of AA-APES is that it still contains nitrogen nutrition. Despite of low P level in lake water, N becomes the limited factor of alga blooms when the ratio of N to P in lake water is lower than in the alga [14].

For the concentration determination, several analytical methods such as turbidimetric, potentiometric, fluorescent tracer, and spectrometric methods are available [15]. Fluorescence methods provide direct measurement and control of a wide array of treatment actives [16–18]. Presently, there are two methods to prepare fluorescent polymers. One is the copolymerization of a monomer containing a fluorescent chromophore and other monomer, the other is chemical modification of polymers by fluorescent groups [19,20]. There exist some reports about the fluorescent scale inhibitor, generally focusing on polyacrylate and poly (maleic acid) [21,22]. Moriarty performed 8-allyloxy-1,3,6-pyrene trisulfonic acid trisodium salt (APTA) fluorescent monomers. Hydrophilic of APTA is strong because of sulfoacid hydrophilic groups [23].

In this paper, a new calcium carbonate scaling inhibitor was studied. The purpose of the present study presents the results of "green" chemicals study that was undertaken to investigate the ability of new inhibitors (Acrylic acid–Oxalic acid–Allypolyethoxy carboxylate (AA-APEM)) to inhibit the scale problems found in cooling water systems, and prepared fluorescent-tagged no phosphate and nitrogen-free inhibitor AA-APEM-APTA by free copolymerization.

2. Experimental

2.1. Materials

8-Hydroxy-1,3,6-pyrene trisulfonic acid trisodium salt (pyranine) was purchased from Xuhua Chemical (Shanghai, China). Allyloxy polyethoxy ether (APEG) was purchased from Zhongshan Chemical (Nanjing, Jiangsu, China). Other reagents such as acrylic acid, oxalic acid, potassium peroxydisulfate, allyl chloride, and ammonium persulfate of AR grade were obtained from Zhongdong Chemical Reagent (Nanjing, Jiangsu, China). Poly (acrylic acid) (PAA, 1800 MW), hydrolyzed polymaleic acid (HPMA, 600 MW), and polyepoxysuccinic acid (PESA, 1500 MW) were of technical grade and supplied by Jiangsu Jianghai Chemical Co. Ltd. Distilled water was used for all the studies.

2.2. Preparation of APEM, APTA, and AA-APEM-APTA

The carboxylic acid functionalization of the surface hydroxyl groups was realized by reaction with oxalic acid (OA). The synthesis procedure of APEM is shown in Fig. 1.

APTA was synthesized according to Moriarty [23]. The product was light yellow in color. Synthesis procedure of APTA from pyranine and allyl chloride is shown in Fig. 2.

Ninety gram (5 mol) distilled water, 7.2 g (0.1 mol) AA, and 16 g (0.03 mol) APEM (the mole ratio of AA and APEM was 4:1) were mixed together in a 250 mL five-neck round-bottomed flask fitted with a thermometer and a magnetic stirrer. The mixture was heated to 70℃ with stirring under nitrogen atmosphere. Around 0.66 g, 1 mmol of APTA (the amount of APTA in the tagged copolymers is 2.5 weight percent) in 20 g distilled water, 1.0 g ammonium persulfate in 20 g distilled water, and 1.0 g sodium metabisulfite in 20 g distilled water were added dropwise in the 250 mL round-bottomed flask over a period of 1.0 h at 70℃. And then, the reactant was heated with stirring at 80℃ for 1.5 h under nitrogen atmosphere. The mixture was subsequently cooled and the polymer was then isolated by successive precipitations in a large volume of acetone. The insoluble product was filtered, collected, and

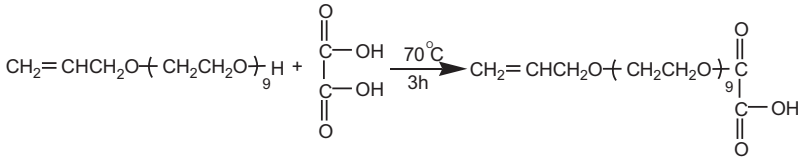

Fig. 1. Preparation of APEM.

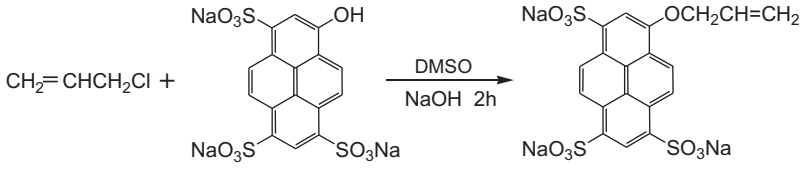

Fig. 2. Preparation of APTA.

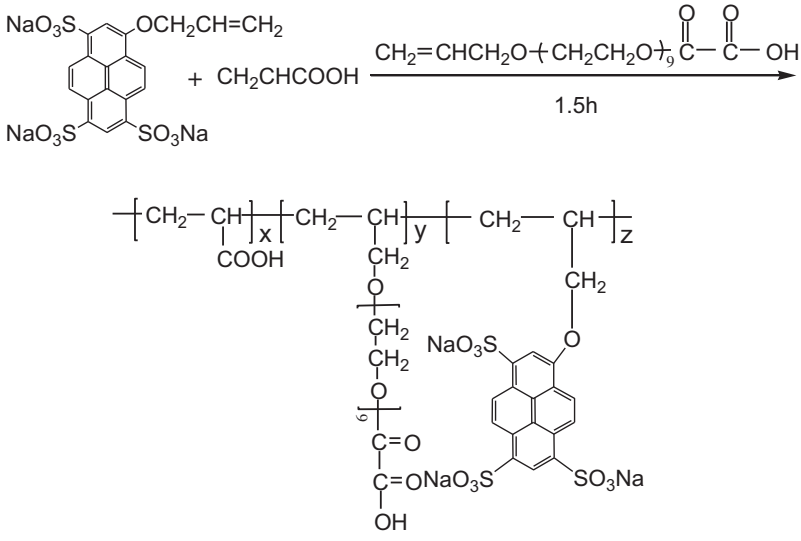

Fig. 3. Preparation of AA-APEM-APTA.

extracted in a soxhlet extractor for 16.0 h to remove the unused AA and APEM. The crude product was dried in a vacuum oven until constant weight, and re-crystallized from water–acetone mixture (3:7 V/V) to remove the residual APTA and gain AA-APEM-APTA as a white solid. The synthesis procedure of AA-APEM-APTA from AA, APEM, and APTA is shown in Fig. 3.

2.3. Measurements

The samples were analyzed using a FT–IR spectroscopy (VECTOR-22, Bruker Co., Germany) in the region of 4,000–500 cm^{-1}. Prior to the measurement, the samples were dried under vacuum until reaching to a constant weight. The dried samples were pressed into the powder, mixed with KBr powder, and then compressed to make a pellet for FT–IR characterization.

X-ray diffraction (XRD) patterns of the $CaCO_3$ crystals were recorded on a Rigaku D/max 2400 X-ray powder diffractometer with Cu Kα (λ = 1.5406) radiation (40 kV, 120 mA).

Scanning electron microscopy (SEM) images were recorded using a field emission scanning electron microscope (S-3400 N HITECH SEM). Prior to imaging by SEM, the scale samples were sputtered with a thin layer of gold. The shape of $CaCO_3$ scale was observed with a transmission electron microscope (TEM, JEM-2100SX, Japan).

Fluorescence measurements were carried out on a luminescence spectrometry (LS-55, Perkin–Elmer, UK) with a xenon lamp as a light.

2.4. Precipitation of calcium carbonate experiments

All precipitation experiments were carried out in flask tests and all inhibitors dosages given below are on a dry-inhibitor basis. Tests of the inhibitors were carried out using supersaturated solutions of $CaCO_3$ at 80 ℃. The solutions were prepared by dissolving the reagent grade $CaCl_2$ and $NaHCO_3$ (Zhongdong Chemical Reagent Co.) in distilled water at equivalent concentrations of 24 milliequivalent/L (cooling water code GB/T 16632-2008). The supersaturation level of the solutions corresponded to a Langelier Index of 2.1. Each inhibition test was carried out in a 500 mL flask immersed in a temperature-controlled bath for 10 h. Precipitation of $CaCO_3$ was monitored by analyzing aliquots of the filtered (0.22 μm) solution for Ca^{2+} ions

using EDTA complexometry as specified in code GB/T 15452-2009. Inhibitor efficiency was calculated from the following equation:

$$\text{Inhibition}\,(\%) = \frac{[Ca^{2+}]_{final} - [Ca^{2+}]_{blank}}{[Ca^{2+}]_{initial} - [Ca^{2+}]_{blank}} \times 100\% \quad (1)$$

where $[Ca^{2+}]_{final}$ and $[Ca^{2+}]_{blank}$ are final calcium concentrations with and without the presence of an inhibitors, respectively, and $[Ca^{2+}]_{initial}$ is the initial calcium concentration.

2.5. Excitation and emission wavelength measurement of APTA and AA-APEM-APTA

Excitation and emission wavelengths of APTA and AA-APEM-APTA were all measured at β_{ex} = 402 nm (10 nm slid width) and β_{em} = 430 nm (5 nm slid width), respectively. The excitation and emission wavelengths were chose the same as the excitation and emission wavelength of pyranine. Approximately, 5×10^{-8} mol/L APTA distilled water solution was prepared and AA-APEM-APTA was dissolve in quantum sufficient distilled water and concentration of APTA in AA-APEM-APTA solution was also 5×10^{-8} mol/L.

2.6. Detection of AA-APEM-APTA fluorescent intensity with different concentration

Use of inert fluorescent tracers and on-line fluorometer provides accurate control of treatment dosage and immediate response to changes in treatment dosage. Fluorescent light is emitted that ought to directly proportional to the dosage of treatment in the water, which translates into reliable control of treatment dosage. A serial concentration of AA-APEM-APTA sample should reflect a corresponding serial of the fluorescence intensity. Prepared 2, 4, 6, 8, 10, 12, 14, 16, and 18 mg/L AA-APEM-APTA aqueous solution samples to estimate AA-APEM-APTA fluorescent intensity response to their concentration.

3. Results and discussion

3.1. FT–IR measurements

The FT–IR spectra of APTA, APEM, and AA-APEM-APTA are exhibited in Fig. 4. APTA (FT–IR, cm^{-1}): 660~880 (C–H plane deformation vibration of aromatic compound), 1,047 (alkyl oxide characteristic absorption of APTA), 1,276 (fragrant ether characteristic absorption), 1,450~1,630 (aromatic compound absorption band), 1,657 (C = C stretching vibration), and 3,449 (O–H stretching vibration). Presently, two bands exist to prove the monomer structure which includes alkyl aryl ether. The 1,743 cm^{-1} strong intensity absorption peak (–C=O) in curve *b* clearly reveals that APEM has been synthesized successfully. The fact that the (–C=C–) stretching vibration at 1,642 cm^{-1} appears in curve *b* but disappears completely in curve *c* reveals that free radical polymerization between AA, APEM, and APTA has happened.

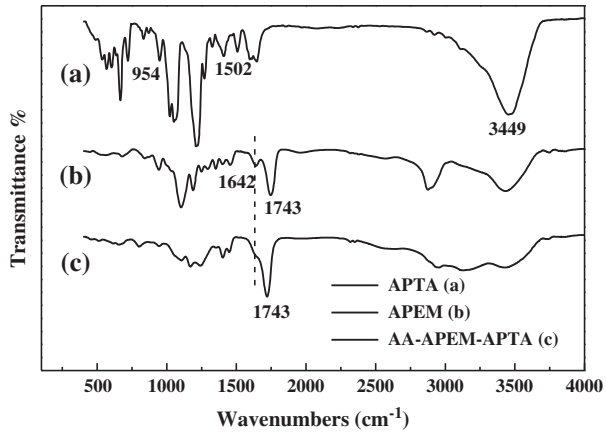

Fig. 4. FT-IR spectra of (a) APTA, (b) APEM, and (c) AA-APEM-APTA.

3.2. Excitation and emission properties of APTA and AA-APEM-APTA

On the basis of the data presented in Figs. 5 and 6, it can be achieved by the figure that excitation and emission wavelengths of APTA and AA-APEM-APTA are 402 and 430 nm, respectively. Excitation spectra

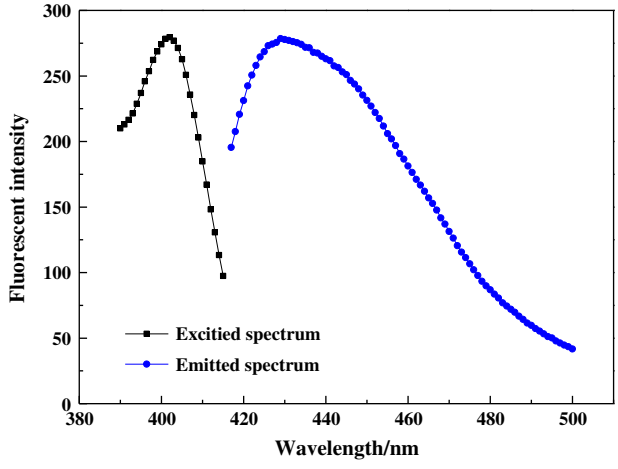

Fig. 5. Excitation and emission wavelength of APTA.

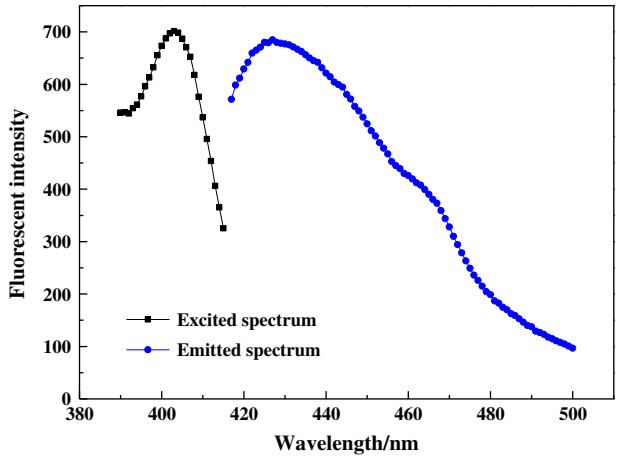

Fig. 6. Excitation and emission wavelength of AA-APEM-APTA.

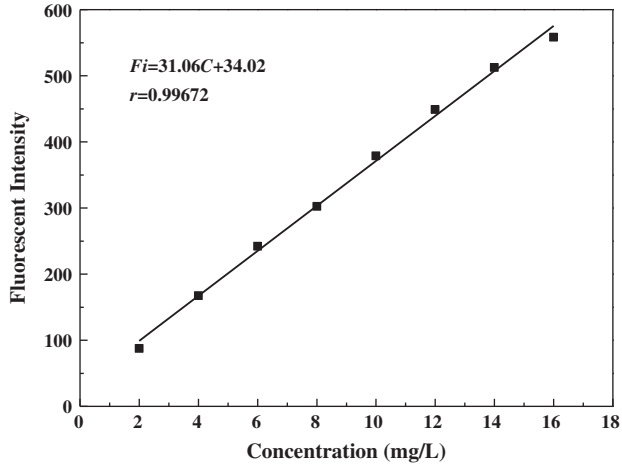

Fig. 7. Linearity of the fluorescence intensity (*Fi*) with the concentration (*C*) of AA-APEM-APTA.

and emission spectra of AA-APEM-APTA show good mirror image relationship as APTA. The fluorescence intensity of AA-APEM-APTA increased compared with APTA after copolymerization because of the formation of hydrogen bonding. The lowest singlet excited states of aromatic carbonyl compounds such as APTA is (n, Π*). The excited state possess (n, φ*) character in non-polar and weakly hydrogen-bonding solvents but they exhibit enhanced (φ*, φ*) character in very polar hydrogen-bonding solvents. (φ*, φ*) states are, or become, the energetically lowest states after copolymerization. Also Rusakowicz have cited evidence that benzophenone and presumably other normally (n, φ*) aromatic carbonyl compounds possess enhanced singlet (φ*, φ*) character in very polar and acidic media. The yields of fluorescence grow in quantity in (φ*, φ*) states than in (n, φ*) states [24].

3.3. Response of fluorescent intensity over a range of AA-APEM-APTA

The result of linearity testing between AA-APEM-APTA fluorescence intensity and their concentration is shown in Fig. 7. Fluorescence intensity was in linear with AA-APEM-APTA concentration in the range 2–18 mg/L which is common dosage scope to the inhibitors. The relationship between AA-APEM-APTA concentration and fluorescence intensity provided exceptionally linear response [correlation coefficient r = 0.99672]. This positive linear relationship can be used to measure AA-APEM-APTA concentration accurately. The detection limit of AA-APEM-APTA is 0.75 mg/L according to the detection limit formula: $D_r = 3\sigma/k$, where σ is 11 times determination of blank solution's standard deviation and k is the slope of calibration curve [25].

3.4. Influence of AA-APEM and AA-APEM-APTA dosage on $CaCO_3$ inhibition

The scale inhibition performance of AA-APEM and AA-APEM-APTA in simulated scale inhibition solution at different concentrations of inhibitor was shown in Fig. 8. For $CaCO_3$ inhibition, AA-APEM-APTA was weakly inferior to AA-APEM, but 70.2% inhibition was obtained at the concentration of 8 mg/L. Compared to AA-APEM-APTA, a most recent effective inhibitor, AA-APEM-APTA had superior ability to inhibit the $CaCO_3$ scale, with

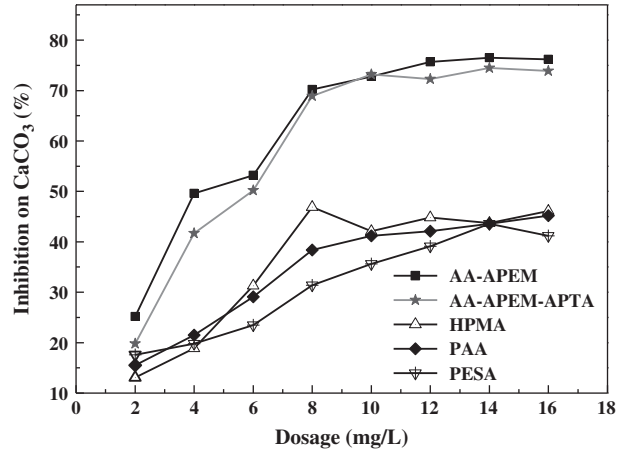

Fig. 8. Scale inhibition of AA-APEM, AA-APEM-APTA, and different commercial inhibitor on $CaCO_3$ at different concentrations of copolymers, respectively.

50.2% inhibition at a level of 6 mg/L, whereas it is 31.3% for HPMA at the same dosage (the best inhibitor among them). So, when compared to these non-phosphorus inhibitors, $CaCO_3$ inhibition of AA-APEM-APTA is much better than that of HPMA, PAA, and PESA at the same dosage. It can be shown that the order of preventing the precipitation from flask tests was AA-APEM > AA-APEM-APTA > HPMA > PAA≈PESA.

Also, we can find that PAA and HPMA contain carboxyl groups and possess molecular structure to AA-APEM-APTA inhibitor but can hardly control $CaCO_3$ scale even at a high dosage. It may be that the side-chain polyethylene (PEG) segments of APEM and carboxyl groups of AA play an important role during the control of calcium carbonate scales. Carboxyl segments and PEG are important parts on matrices of AA-APEM. Also, there are some carboxyls in the molecular chains of the copolymer which have the complexation function to Ca^{2+} [26]. The functional groups of anti-scalant exhibit a significant impact on their inhibitory power in terms of controlling the scale precipitation.

3.5. Characterization of calcium carbonate scale

In order to better analyze the impact of AA-APEM-APTA on the growth of $CaCO_3$ crystal, the experiment used AA-APEM-APTA as scale inhibitor, and the collected $CaCO_3$ crystal was characterized by SEM and XRD analyses. The $CaCO_3$ collected from the experiments without the addition of AA-APEM-APTA showed the characteristic of regular shaped rhombohedra, and the particles' size was uniform (Fig. 9(a)). When the AA-APEM-APTA concentration increased to 6 mg/L, sharp edges and acute corners of the crystals disappeared completely (Fig. 9(b)). From a thermodynamic point of view, the obtained crystal morphology could minimize the free enthalpy of the crystal which was the sum of the products of surface energy and area of all exposed faces [27,28].

Fig. 10 showed the TEM images of the precipitates after 24 h crystallization and precipitation with (Fig. 10(b)) or without (Fig. 10(a)) the addition of AA-APEM-APTA. The precipitates collected from the experiments without addition of AA-APEM-APTA showed the characteristic regular shaped rhombohedra and the particles' size was uniform (Fig. 10(a)).

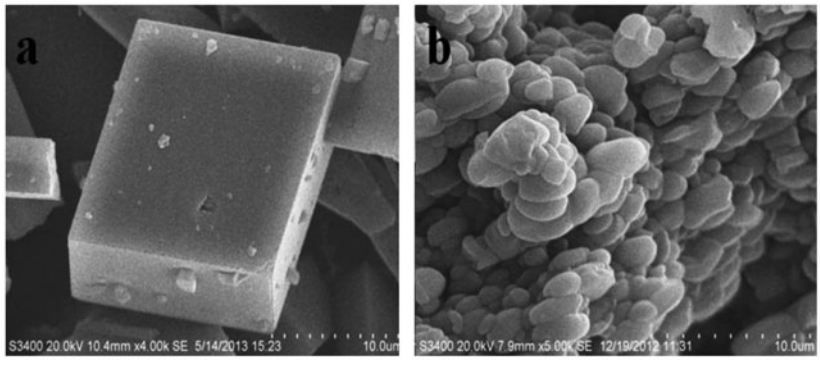

Fig. 9. SEM photographs for (a) the $CaCO_3$ and (b) with the presence of AA-APEM-APTA, 6 mg/L.

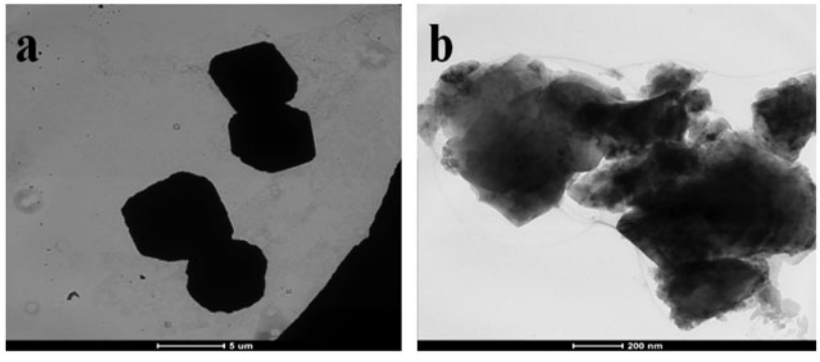

Fig. 10. (a) TEM photographs for the $CaCO_3$ and (b) with the presence of AA-APEM-APTA, 6 mg/L.

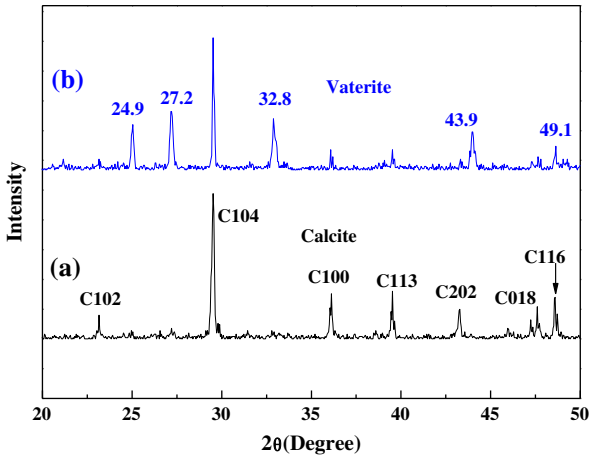

Fig. 11. XRD image of the $CaCO_3$ crystal formed (a) in the absence of AA-APEM-APTA and (b) with the presence of AA-APEM-APTA, 6 mg/L.

But when 6 mg/L AA-APEM-APTA concentration was added, loose and soft particle was visible in the TEM image (Fig. 10(b)). The mechanism of the shape process is similar to the SEM.

In the absence of AA-APEM-APTA copolymer, calcite is the main crystal form (Fig. 11(a)). Fig. 11(b) shows the XRD spectrum for $CaCO_3$ precipitate in the presence of AA-APEM-APTA copolymer, while one could clearly observe a series of quite strong diffraction peaks of 2θ at 24.9˚, 27.2˚, 32.8˚, 43.9˚, 49.1˚ corresponding to Miller indices (110), (112), (114), (300), and (118), typical of vaterite (JCPDS No. 33-0286 in space group $P6_3/mmc$) [29–31]. These results indicate that in the presence of the AA-APEM-APTA copolymer the $CaCO_3$ precipitate is the mixture of calcite and vaterite. It is well known that calcite is the most thermodynamically stable, and vaterite is the least stable form in the three polymorphic forms of $CaCO_3$ [32]. As a result, the impact on heat transfer can be prevented and the scale inhibition effect can be acquired.

4. Conclusions

In this study, the effect of a copolymer on the calcium carbonate inhibition was investigated. Fluorescent-tagged no carbonate and nitrogen-free calcium carbonate inhibitor AA-APEM-APTA was successfully synthesized by free polymerization of AA, APEM, and APTA. FT-IR identified that AA-APEM-APTA has the expected structures. It can be concluded that the order of preventing the precipitation from flask tests was AA-APEM > AA-APEM-APTA > HPMA > PAA≈PESA.

Good relationship between AA-APEM-APTA fluorescent intensity and its dosage (the correlation coefficient r = 0.99672) ensures that AA-APEM-APTA is a valuable indicator for cooling water system performance. SEM images indicate that AA-APEM-APTA changes highly the morphology and size of calcium carbonate crystals during the inhibition process. The TEM mechanism of the scale/shape effect process is similar to the SEM. XRD analysis shows that some calcite crystals are changed into another $CaCO_3$ structure, formed in vaterite after adding AA-APEM-APTA.

Acknowledgments

This work was supported by the Prospective Joint Research Project of Jiangsu Province (BY2012196); the National Natural Science Foundation of China (51077013); special funds for Jiangsu Province Scientific and Technological Achievements Projects of China (BA2011086); Scientific Innovation Research Foundation of College Graduate in Jiangsu Province (CXLX13-107、CXZZ13-0091); and program for Training of 333 High-Level Talent, Jiangsu Province of China (BRA2010033).

References

[1] J.K. Kim, R. Smith, Cooling water system design, Chem. Eng. Sci. 56 (2001) 3641–3658.
[2] H.M. Zeng, J.Y. Lin, C.S. Ye, L.H. Tong, X.L. Chen, F. Yu, Ion exchange softening and alkalization treatment for zerodischarge of circulating cooling water, J. Electron. Anal. Appl. 1 (2009) 6–10.
[3] D. Liu, F. Hui, J. Lédion, F.T. Li, Study of the scaling formation mechanism in recycling water, Environ. Technol. 32 (9) (2011) 1017–1030.
[4] M.A.-H. Luai, Q. Abdul, A.A.-O. Dhawi, Calcium sulfate scale deposition on coated carbon steel and titanium, Desalin. Water Treat. 51 (2013) 2521–2528.
[5] F. Liu, X.H. Lu, W. Yang, J.J. Lu, H.Y. Zhong, X. Chang, C.C. Zhao, Optimizations of inhibitors compounding and applied conditions in simulated circulating cooling water system, Desalination 313 (2013) 18–27.
[6] C.E. Fu, Y.M. Zhou, G.Q. Liu, J.Y. Huang, W. Sun, W.D. Wu, Inhibition of $Ca_3(PO_4)_2$, $CaCO_3$, and $CaSO_4$ precipitation for industrial recycling water, Ind. Eng. Chem. Res. 50 (2011) 10393–10399.
[7] A.O. Saleah, A.H. Basta, Evaluation of some organic-based biopolymers as green inhibitors for calcium sulfate scales, Environmentalist 28 (2008) 421–428.
[8] P. Kjellin, X-ray diffraction and scanning electron microscopy studies of calcium carbonate electrodeposited on a steel surface, Coll. Surfaces A: Physicochem Eng. Aspects 212 (2003) 19–26.
[9] Syaiful SuharsoTeguh BuhaniE. Bahri, Gambier extracts as an inhibitor of calcium carbonate ($CaCO_3$) scale formation, Desalination 265 (2011) 102–106.

[10] A.A. Koelmans, H.A. Vander, L.M. Knijff, R.H. Aalderink, Integrated modelling of eutrophication and organic contaminant fate & effects in aquatic ecosystems, Water Res. 35 (15) (2001) 3517–3536.
[11] S.M. Kessler, Analyses the performance of a next generation phosphate inhibitor for industrial water application, Hydrocarbon Eng. 8 (2003) 66–72.
[12] S.M. Kessler, Advanced scale control technology for cooling water systems. TX, Annual conference of national association of corrosion engineerings, Houston, 2002, p. 02402.
[13] S.M. Kessler, Phosphate inhibition efficacy for the twenty first century. TX, Annual conference of national association of corrosion engineerings, Houston, 2004, p. 04076.
[14] H. Fang, J.M. Mo, Reactive nitrogen increasing: a threat to our environment, Ecol. Environ. 15 (1) (2006) 164–168. (In Chinese).
[15] A. Yuchi, Y. Gotoh, S. Itoh, Potentiometry of effective concentration of polyacrylate as scale inhibitor, Anal. Chim. Acta 594 (2007) 199–203.
[16] Z.Q. Wu, L.Z. Meng, Progress in fluorescent polymers, Progre. Chem. 19 (9) (2007) 1381–1392. (In Chinese).
[17] R. Gatti, C. Lotti, Development and validation of a pre-column reversed phase liquid chromatographic method with fluorescence detection for the determination of primary phenethylamines in dietary supplements and phytoextracts, J. Chromatogr. A 1218 (2011) 4468–4473.
[18] R. Martínez-Máñez, F. Sancenón, Fluorogenic and chromogenic chemosensors and reagents for anions, Chem. Rev. 103 (2003) 4419–4476.
[19] A. Nagai, K. Kokado, J. Miyake, Y. Cyujo, Thermoresponsive fluorescent water-soluble copolymers containing BODIPY dye: inhibition of H-Aggregation of the BODIPY units in their copolymers by LCST, J. Polym. Sci., Part A: Polym. Chem. 48 (2010) 627–634.
[20] H.C. Chu, Y.H. Lee, S.J. Hsu, P.J. Yang, A. Yabushita, H.C. Lin, Novel reversible chemosensory material based on conjugated side-chain polymer containing fluorescent pyridyl receptor pendants, J. Phys. Chem. B 115 (2011) 8845–8852.
[21] J.D. Morris, B.E. Moriarty, M.L. Wei, P.G. Murray, J.L. Reddinger, U.S. Patent 6645428B1, (2003).
[22] M. Kira, N. Kobayashi, U.S. Patent 5624995, (1997).
[23] B.E. Moriarty, J.E. Hoots, D.P. Workman, J.P. Rasimas, U.S. Patent 6312644, (2001).
[24] R. Richard, G.W. Byers, P.A. Leermakers, Electronically excited aromatic carbonyl compounds in hydrogen bonding and acidic media, J. Am. Chem. Soc. 93 (13) (1971) 3263–3266.
[25] L.J. Gao, J.Y. Feng, B. Jin, Q.N. Zhang, T.Q. Liu, Y.Q. Lun, Z.J. Wu, Carbazole and hydroxy groups-tagged poly(aspartic acid) scale inhibitor for cooling water systems, Chem. Lett. 40 (2011) 1392–1394.
[26] X.H. Qiang, Z.H. Sheng, H. Zhang, Study on scale inhibition performances and interaction mechanism of modified collagen, Desalination 309 (2013) 237–242.
[27] M.M. Reddy, A.R. Hoch, Calcite crystal growth rate inhibition by polycarboxylic acids, J. Colloid. Interface. Sci. 235 (2001) 365–370.
[28] J.M. Didymus, S. Mann, W.J. Benton, I.R. Collins, Interaction of poly (α,β-aspartate) with octadecylamine monolayers: adsorption behavior and effects on $CaCO_3$ crystallization, Langmuir 11 (1995) 3130–3136.
[29] N.V. Vagenas, A. Gatsouli, C.G. Kontoyannis, Quantitative analysis of synthetic calcium carbonate polymorphs using FT-IR spectroscopy, Talanta 59 (2003) 831–836.
[30] Q.W. Meng, D.Z. Chen, L.W. Yue, J.L. Fang, H. Zhao, L.L. Wang, Hyperbranched polyesters with carboxylic or sulfonic acid functional groups for crystallization modification of calcium carbonate, Macromol. Chem. Phys. 208 (2007) 474–484.
[31] L.L. Wang, Z.L. Meng, Y.L. Yu, Q.W. Meng, D.Z. Chen, Synthesis of hybrid linear-dendritic block copolymers with carboxylic functional groups for the biomimetic mineralization of calcium carbonate, Polymer 49 (2008) 1199–1210.
[32] S.I. Kuriyavar, R. Vetrivel, S.G. Hegde, A.V. Ramaswamy, D. Chakrabarty, S. Mahapatra, Insights into the formation of hydroxyl ions in calcium carbonate: temperature dependent FTIR and molecular modelling studies, J. Mater. Chem. 10 (2000) 1835–1840.